A physically motivated L_2 norm for compressible flow

By S. R. Gomez

L_2 norms are useful for measuring the strength of a disturbance or defining inner products to compare state vectors within a fluid domain. They are also necessary to define commonly used data-driven flow decompositions like the proper orthogonal decomposition (POD) and spectral proper orthogonal decomposition (SPOD) and equation-based approaches like transient growth theory, resolvent analysis, and adjoint methods. For compressible ideal gas flows, researchers often use the Chu energy norm (Chu 1965) as a measure of the disturbance energy. However, this norm is quadratic in both the density and the specific internal energy, e, limiting its interpretability. By introducing the new variable $c = \sqrt{e}$, a total energy norm is defined based on the kinetic energy and c^2. This norm measures the mean specific total energy of a fluctuation in a single-species ideal gas. The new norm is applied to near-wall POD modes and the resolvent analysis of supersonic wall-bounded turbulent flows and compared with the Chu norm.

1. Introduction

In fluid applications, it is desirable to have a measure to quantitatively compare the noise generation, temporal evolution, or mitigation of a flow disturbance within a domain, Ω. A useful measure is the L_2 norm, $\|\boldsymbol{q}\|_2^2 = \langle \boldsymbol{q}, \boldsymbol{q} \rangle_2$, defined by the inner product $\langle \boldsymbol{q}_1, \boldsymbol{q}_2 \rangle_2 = \int_\Omega \boldsymbol{q}_1^*(\boldsymbol{x}) \mathbf{W}(\boldsymbol{x}) \boldsymbol{q}_2(\boldsymbol{x}) d\boldsymbol{x}$, *, where denotes a complex-conjugate, for a positive-definite operator $\mathbf{W}$. A useful aspect of the L_2 norm and its associated inner product is that they enable Schmidt decompositions (or singular value decompositions (SVD)) of linear operators and matrices as $\boldsymbol{A} = \sum_i \sigma_i \boldsymbol{l}_i \boldsymbol{r}_i^*$, where σ_i are the singular values, and $\boldsymbol{l}_i$ and $\boldsymbol{r}_i$ are the left and right singular vectors, respectively. This decomposition identifies the nonzero $\boldsymbol{r}$ that maximizes the Rayleigh quotient, $\sigma^2 = \|\boldsymbol{A}\boldsymbol{r}\|_2^2 / \|\boldsymbol{r}\|_2^2$, as the leading right singular vector, $\boldsymbol{r}_1$, with $\max \sigma = \sigma_1$. The SVD enables the identification of data-driven orthonormal bases that describe the flow statistics and identify coherent structures with methods like the proper orthogonal decomposition (POD) (Lumley 1967; Berkooz *et al.* 1993; Moin & Moser 1989) and spectral proper orthogonal decomposition (SPOD) (Picard & Delville 2000; Sieber *et al.* 2016). The optimization of the Rayleigh quotient forms the basis of resolvent analysis where one seeks the unit-norm forcing that leads to the largest amplification in the linearized Navier–Stokes equations (NSE) (McKeon & Sharma 2010) and transient growth analysis where one seeks the initial condition that is most linearly amplified in some time horizon (Hanifi *et al.* 1996; Schmid & Henningson 2001). The associated inner product also enables the definition of an adjoint which enables various optimization strategies, the study of adjoint eigenmodes (Schmid & Henningson 2001), and a way to identify projection coefficients for an appropriately chosen basis flow reconstruction (Taira *et al.* 2017).

For an incompressible fluid, a natural choice for the L_2 norm is the specific kinetic energy, $\boldsymbol{u}' \cdot \boldsymbol{u}'/2$, within Ω, where $\boldsymbol{u}$ is the velocity vector and $'$ denotes a fluctuation. In a compressible single-species ideal gas flow, the relevant measure of energy is the total

specific energy, $e_t = \boldsymbol{u} \cdot \boldsymbol{u}/2 + e$, where e is the specific internal energy. However, this measure poses a problem in the definition of an L_2 norm relevant for the compressible energy because e_t has a quadratic term in $\boldsymbol{u}$ and a linear term in e. Recognizing this, Chu (1965) defined a norm using $E_C = \int_\Omega \left[\overline{\rho}\boldsymbol{u}' \cdot \boldsymbol{u}'/2 + (\gamma - 1)\overline{e}\rho'^2/(2\overline{\rho}) + \overline{\rho}e'^2/(2\overline{e})\right] d\boldsymbol{x}$, where γ is the ratio of specific heats, ρ is the density, and bars denote averages in time and homogeneous directions. The first term is a mean-density weighted kinetic energy, while the second and third term are interpreted as a potential energy or acoustic energy. It will be shown in section 2.2 that the last term is actually twice the linearized internal energy contribution. Hanifi *et al.* (1996) independently determined the weights in the integrand of E_C by enforcing that compressive work terms do not contribute to the time evolution of E_C. The Chu norm has been used for a number of compressible studies involving POD (Towne *et al.* 2018), SPOD (Schmidt *et al.* 2018), resolvent analysis (Bae *et al.* 2020; Karban *et al.* 2020), and transient growth analysis (Hanifi *et al.* 1996), to name a few. Other norms have been applied to compressible flows, with George & Sujith (2011) summarizing a few relying on a quadratic form between the velocities and thermodynamic variables and demonstrating some desirable properties regarding the Chu norm and the Euler equations.

Despite the interpretation of the compressible terms as a potential energy, the terms appearing within the integrand of E_C are not quantities that appear in the energy conservation equations. To remedy this, consider the change of variables proposed by Fan *et al.* (2022) through $c = \sqrt{e}$ as a speed proportional to the speed of sound for a single-species ideal gas. Introducing this into e_t and averaging results in $\overline{e}_t = \left(\overline{\boldsymbol{u}} \cdot \overline{\boldsymbol{u}}/2 + \overline{c}^2\right) + \left(\overline{\boldsymbol{u}' \cdot \boldsymbol{u}'}/2 + \overline{c'c'}\right)$, where the first two terms are here defined as the specific mean kinetic energy and specific mean internal energy, respectively, while the last two are the specific turbulent kinetic energy (TKE) and specific turbulent internal energy, respectively. This change of variables has been shown to form an alternative interpretation of the energy transfer mechanisms in turbulent wall-bounded flows (Fan *et al.* 2022; Fan & Li 2023) by relating terms within the kinetic and internal energy conservation equations. A useful aspect of introducing c is that it enables a quadratic form for e_t. As such, a proposed physically relevant L_2 norm is $E_T = \int_\Omega \overline{\rho}[\boldsymbol{u}' \cdot \boldsymbol{u}'/2 + c'c']d\boldsymbol{x}$, which will be discussed in the remainder of this report. The nonlinear change of variables can also affect the linearized NSE because of differences in the mean state (Karban *et al.* 2020). This will then necessitate a new resolvent operator when c is introduced. While Favre decompositions may be more advantageous for compressible flows, this study will apply the different norms to Reynolds decompositions in line with the original description of the Chu norm and subsequent analytical considerations (Chu 1965; George & Sujith 2011). Although some linear studies do consider conservative state variables (Mettot *et al.* 2014; Karban *et al.* 2020), and thus Favre decomposition for the mean linearization, the states herein will be composed of ρ, $\boldsymbol{u}$, and e or c, thus necessitating a Reynolds decomposition to describe the mean state and its fluctuations.

The rest of the report is organized as follows. Section 2 explains the governing equations, the new norms used herein, the POD, and the resolvent analysis framework using c as opposed to e. Additionally, the temporal evolution of the Chu and total energy norms for a simple disturbance in a quiescent fluid is addressed to highlight differences in the measured disturbance energy growth. Section 3 compares the different modes and gains using the different norms for a near-wall POD mode, a near-wall resolvent mode, and an acoustic resolvent mode. Implications for modeling are discussed. Conclusions and future work are presented in Section 4.

2. Methodology

This study considers planar supersonic flows consisting of a turbulent boundary layer (TBL) and channels evolving over time, t, as single-species calorically perfect ideal gases. Here, the velocity vector is $\boldsymbol{u} = (u, v, w)$, with u, v, and w denoting the streamwise, wall-normal, and spanwise velocity components, respectively; position is $\boldsymbol{x} = (x, y, z)$, with x, y, and z denoting the streamwise, wall-normal, and spanwise coordinates, respectively. Following Fan *et al.* (2022)'s observations that using c rather than e results in a more interpretable energy exchange between the mean kinetic energy, TKE, mean internal energy, and turbulent internal energy along with the need for a quadratic description of the compressible energy, c will now be considered as a nonlinear coordinate transformation to enable an energy norm resembling the total energy.

Here, two different state vectors are considered: $\boldsymbol{q}_e = [u, v, w, e, \rho]$ and $\boldsymbol{q}_c = [u, v, w, c, \rho]$. Hereafter, variables are normalized with a velocity scale, u_s, length scale, ℓ_s, density scale, ρ_s, dynamic viscosity scale, μ_s, and temperature scale, T_s. For variables with a $+$ subscript, $u_s = u_\tau = \sqrt{\tau_w/\rho_w}$, $\ell_s = \mu_w/(\rho_w u_\tau)$, $\mu_s = \mu_w$, $\rho_s = \rho_w$, and $T_s = T_w$, where the subscript w denotes wall quantities. The scales define the Reynolds number, $Re = u_s \ell_s \rho_s / \mu_s$. For the channel flow, the Mach number is $Ma = u_b/a_w$, where u_b is the bulk velocity and a_w is the speed of sound at the wall. For the boundary layer, $Ma = u_\infty/a_\infty$, where u_∞ is the freestream velocity and a_∞ is the freestream speed of sound. In what follows, the governing equations are described using either e or c. The norms used herein will then be discussed in more detail along with an example of their temporal evolution. Finally, brief discussions of POD and resolvent analysis will be given.

2.1. *Governing equations and nomenclature*

The flows satisfy the compressible NSE for a single-species calorically perfect ideal gas,

$$\frac{\partial \rho}{\partial t} + \boldsymbol{\nabla} \cdot (\rho \boldsymbol{u}) = 0, \tag{2.1}$$

$$\rho\left(\frac{\partial \boldsymbol{u}}{\partial t} + (\boldsymbol{\nabla}\boldsymbol{u})\boldsymbol{u}\right) = -\boldsymbol{\nabla} p + \frac{1}{Re}\boldsymbol{\nabla} \cdot \tau + \rho b \boldsymbol{e}_x, \tag{2.2}$$

$$\rho\left(\frac{\partial e}{\partial t} + \boldsymbol{\nabla} e \cdot \boldsymbol{u}\right) = -p\boldsymbol{\nabla} \cdot \boldsymbol{u} + \frac{\gamma}{Re\,\mathrm{Pr}}\boldsymbol{\nabla} \cdot (\mu \boldsymbol{\nabla} e) + \frac{1}{Re}\tau : \boldsymbol{\nabla}\boldsymbol{u}, \tag{2.3}$$

$$\rho\left(\frac{\partial c}{\partial t} + \boldsymbol{\nabla} c \cdot \boldsymbol{u}\right) = -\frac{p}{2c}\boldsymbol{\nabla} \cdot \boldsymbol{u} + \frac{\gamma}{Re\,\mathrm{Pr}}\frac{1}{2c}\boldsymbol{\nabla} \cdot \left(\mu \boldsymbol{\nabla} c^2\right) + \frac{1}{Re}\frac{1}{2c}\tau : \boldsymbol{\nabla}\boldsymbol{u}, \tag{2.4}$$

where Eqs. (2.3) and (2.4) are mathematically equivalent. Here, $\mathrm{Pr} = .7$ is the Prandtl number, ρ is the density, $b\boldsymbol{e}_x$ is a driving body force, $\gamma = 1.4$ is the ratio of specific heats, μ is the dynamic viscosity, p is the pressure, and τ is the shear stress tensor. Also, $p = (\gamma - 1)\rho e = (\gamma - 1)\rho c^2$ due to the ideal gas law, and $\tau = \mu\big(\boldsymbol{\nabla}\boldsymbol{u}^T + \boldsymbol{\nabla}\boldsymbol{u} - 2/3\boldsymbol{\nabla} \cdot \boldsymbol{u}\mathcal{I}\big)$, where $\mathcal{I}$ is an identity tensor. The viscosity follows Sutherland's law such that $\mu(T) = (T)^{3/2}(1 + S/T_s)/(T + S/T_s)$, where T is the temperature and $S = 110.4\mathrm{K}$ is the Sutherland temperature. The walls are treated as isothermal where the no-slip and no-penetration conditions are applied. The channel flows are driven by b, while the TBL is driven by the freestream velocity without a driving b.

This study will make use of both Reynolds decompositions where $f = \overline{f} + f'$ and Favre decompositions where $f = \widetilde{f} + f''$ for an instantaneous quantity f. $\overline{f}$ is an average over time and homogeneous directions, and $\widetilde{f} = \overline{\rho f}/\overline{\rho}$ is the Favre average. In the wall-bounded flows, it is assumed the flows are statistically stationary and x and z are homogeneous directions such that $\overline{f} = \overline{f}(y)$ and $\widetilde{f} = \widetilde{f}(y)$.

2.2. *Definition of norms used*

As mentioned before, compressible flows have historically used L_2 norms to define the energy of fluctuations in $\boldsymbol{q}_e$, resulting in energy definitions with quadratic dependencies on e' (or equivalently T') and ρ'. Here, the Chu norm is given by

$$\|\boldsymbol{q}'_e\|^2_C = \int_\Omega \left[\frac{\overline{\rho}}{2}\boldsymbol{u}'\cdot\boldsymbol{u}' + A\rho'^2 + Be'^2\right] d\boldsymbol{x} = \int_\Omega \boldsymbol{q}'^T_e \mathbf{W}_C \boldsymbol{q}'_e d\boldsymbol{x}, \tag{2.5}$$

where $A = (\gamma-1)\overline{e}/(2\overline{\rho})$, $B = \overline{\rho}/(2\overline{e})$, and Ω is the fluid domain. The first term describes the kinetic energy of the fluctuation, while the second and third term define energy terms for the density and temperature fluctuations. The coefficients A and B are defined such that the time evolution of $\|\boldsymbol{q}'_e\|^2_C$ omits any compressive work terms (Hanifi *et al.* 1996). In a similar fashion, a Chu-like energy norm can be defined for $\boldsymbol{q}'_c$ as

$$\|\boldsymbol{q}'_c\|^2_{C_2} = \int_\Omega \left[\frac{\overline{\rho}}{2}\boldsymbol{u}'\cdot\boldsymbol{u}' + A_2\rho'^2 + 2\overline{\rho}c'^2\right] d\boldsymbol{x} = \int_\Omega \boldsymbol{q}'^T_c \mathbf{W}_{C_2} \boldsymbol{q}'_c d\boldsymbol{x}, \tag{2.6}$$

where $A_2 = (\gamma-1)\overline{c}^2/(2\overline{\rho})$. Considering the mean specific total energy, $\overline{e_t} = \overline{\boldsymbol{u}\cdot\boldsymbol{u}}/2 + \overline{e} = \overline{\boldsymbol{u}}\cdot\overline{\boldsymbol{u}}/2 + \overline{c}^2 + \overline{\boldsymbol{u}'\cdot\boldsymbol{u}'}/2 + \overline{c'c'}$, it is clear that the norm in Eq. (2.6) has twice the turbulent internal energy along with an additional density term relating the acoustic energy. While useful, the Chu energy norm does not represent a measure of the mean total kinetic and internal energy of the fluctuations.

As an alternative, by making use of c and the form of the turbulent internal energy, a new L_2 norm can be defined as

$$\|\boldsymbol{q}'_c\|^2_T = \int_\Omega \left[\frac{\overline{\rho}}{2}\boldsymbol{u}'\cdot\boldsymbol{u}' + \overline{\rho}c'^2\right] d\boldsymbol{x} = \int_\Omega \boldsymbol{q}'^T_c \mathbf{W}_T \boldsymbol{q}'_c d\boldsymbol{x}. \tag{2.7}$$

Eq. (2.7) has the interpretation of being a density-weighted $\overline{e_T}$, where $\overline{e_T} = \overline{\boldsymbol{u}'\cdot\boldsymbol{u}'}/2 + \overline{c'c'}$ is the specific turbulent total energy. By introducing a linearization of c, a total energy norm can be defined for $\boldsymbol{q}_e$ through $c' = e'/(2\sqrt{\overline{e}})$. The total energy norm for $\boldsymbol{q}_e$ is then

$$\|\boldsymbol{q}'_e\|^2_{T_2} = \int_\Omega \left[\frac{\overline{\rho}}{2}\boldsymbol{u}'\cdot\boldsymbol{u}' + \frac{\overline{\rho}}{4\overline{e}}e'^2\right] d\boldsymbol{x} = \int_\Omega \boldsymbol{q}'^T_e \mathbf{W}_{T_2} \boldsymbol{q}'_e d\boldsymbol{x}, \tag{2.8}$$

where the weight on e'^2 is $B/2$ from Eq. (2.7).

However, strictly speaking, $\|\boldsymbol{q}'_c\|_T$ and $\|\boldsymbol{q}'_e\|_{T_2}$ are only positive-semidefinite, unlike $\|\boldsymbol{q}'_c\|_{C_2}$ or $\|\boldsymbol{q}'_e\|_C$, because they lack a ρ'^2 term. That is, for $\boldsymbol{q}'_c = [0,0,0,0,\rho]$, $\|\boldsymbol{q}'_c\|_T = 0$, whereas $\|\boldsymbol{q}'_c\|_{C_2} > 0$ and similar for $\boldsymbol{q}'_e$. However, a scenario where both $\boldsymbol{u}'$ and c' are zero while ρ' is nonzero in Ω is not possible because ρ' will create p' that needs to be balanced with $\boldsymbol{u}'$ in the momentum equation. Thus, for the vector space of allowed $\boldsymbol{q}'_c$ and $\boldsymbol{q}'_e$ by the NSE, $\|\boldsymbol{q}'_c\|_T$ and $\|\boldsymbol{q}'_e\|_{T_2}$ are positive-definite. Alternatively, the total energy norm can also be shown to be positive-definite if the state is instead defined as $\boldsymbol{q}_p = [u, v, w, p, \rho]$. Replacing c' with the linearized equation of state creates a norm that is now quadratic in $\boldsymbol{u}'$, p', and ρ' with an integrand that is positive.

Finally, comparisons will also be made with the kinetic energy semi-norm

$$\|\boldsymbol{q}'\|^2_K = \int_\Omega \frac{\overline{\rho}}{2}\boldsymbol{u}'\cdot\boldsymbol{u}' d\boldsymbol{x} = \int_\Omega \boldsymbol{q}'^T \mathbf{W}_K \boldsymbol{q}' d\boldsymbol{x}, \tag{2.9}$$

using $\boldsymbol{q}'_e$ and $\boldsymbol{q}'_c$. In Section 3, the different norms will be color coded following Table 1.

It can be instructive to consider energy measured by the three different norms for the vortical, entropic, and acoustic modes introduced by Kovasznay (1953) for an inviscid

State vector	Norm	Color
$\boldsymbol{q}_c = [u, v, w, c, \rho]$	total energy	
$\boldsymbol{q}_e = [u, v, w, e, \rho]$	total energy	
$\boldsymbol{q}_c = [u, v, w, c, \rho]$	Chu energy	
$\boldsymbol{q}_e = [u, v, w, e, \rho]$	Chu energy	
$\boldsymbol{q}_c = [u, v, w, c, \rho]$	kinetic energy	
$\boldsymbol{q}_e = [u, v, w, e, \rho]$	kinetic energy	

TABLE 1. The state vectors and norms used herein.

steady freestream flow. For the vortical mode with $\boldsymbol{q}'_v = [u'_v, v'_v, w'_v, 0, 0]$ where $\boldsymbol{\nabla}\cdot\boldsymbol{u}'_v = 0$, $\|\boldsymbol{q}_v\|_C = \|\boldsymbol{q}_v\|_{T_2} = \|\boldsymbol{q}_v\|_K$. For the entropic mode with $\boldsymbol{q}'_s = [0, 0, 0, e'_s, -\overline{\rho}e'_s/\overline{e}]$, $\|\boldsymbol{q}_s\|_K = 0$, $\|\boldsymbol{q}_s\|_C^2 = 2\gamma\|\boldsymbol{q}_s\|_{T_2}^2$. Finally, for the acoustic mode with $\boldsymbol{q}'_a = [u'_a, v'_a, w'_a, e'_a, (1-\gamma)\overline{e}\rho'/\overline{\rho}]$ where $\boldsymbol{\nabla} \wedge \boldsymbol{u}'_a = \boldsymbol{0}$, $\|\boldsymbol{q}'_a\|_C^2 = \|\boldsymbol{q}'_a\|_K^2 + 1/2(\gamma)/(\gamma-1)\overline{\rho}/\overline{T}\int_\Omega e_a'^2 d\boldsymbol{x}$ and $\|\boldsymbol{q}'_a\|_{T_2}^2 = \|\boldsymbol{q}'_a\|_K^2 + 1/4\overline{\rho}/\overline{T}\int_\Omega e_a'^2 d\boldsymbol{x}$. This simple example illustrates that the Chu norm weighs the energy of the entropic and acoustic modes more heavily than the total energy norm does. For the acoustic modes, the contribution from e' and ρ' to the Chu norm is 7 times larger than the contribution of these components to the total energy norm for $\gamma = 1.4$.

2.3. *Temporal evolution of the Chu norm and total energy norm*

A classic result is that the total energy of an enclosed system is a conserved quantity in the absence of body forces, heat sources, and heat transfer at the boundaries. Consider a simple system of a steady, quiescent fluid with $\overline{\boldsymbol{u}} = \boldsymbol{0}$, $\overline{e} = e_0$, $\overline{c} = \sqrt{e_0}$, $\overline{\rho} = \rho_0$, and $\overline{p} = (\gamma-1)\rho_0 e_0$ with periodic boundaries with a disturbance $\epsilon\boldsymbol{q}'_e$ with $\epsilon \ll 1$. This system was studied by Chu (1965) and George & Sujith (2011) to show properties of $\|\boldsymbol{q}_e\|_C$. The conserved total energy of the disturbance is $e'_t = \boldsymbol{u}'\cdot\boldsymbol{u}'/2 + e'$, which is not the quadratic form in the integrand of Eq. (2.7) and combines terms of $\mathcal{O}(\epsilon)$ and $\mathcal{O}(\epsilon^2)$. For the integrand in Eq. (2.7), $e_T = \boldsymbol{u}'\cdot\boldsymbol{u}'/2 + c'^2$, it can be shown that

$$\begin{aligned}\rho_0\partial_t e_T = &-\frac{p_0}{c_0}\boldsymbol{\nabla}\cdot(c'\boldsymbol{u}') + \frac{2\gamma\mu_0 c_0}{Re\,\mathrm{Pr}}(\boldsymbol{\nabla}\cdot(c'\boldsymbol{\nabla}c')) + \frac{1}{Re}\boldsymbol{\nabla}\cdot(\tau'\boldsymbol{u}')\\ &-\frac{2\gamma\mu_0 c_0}{Re\,\mathrm{Pr}}(\boldsymbol{\nabla}c'\cdot\boldsymbol{\nabla}c') - \frac{1}{Re}\tau' : \boldsymbol{\nabla}\boldsymbol{u}' - \left(\frac{p_0}{c_0}\boldsymbol{\nabla}c' + \frac{p_0}{\rho_0}\boldsymbol{\nabla}\rho'\right)\cdot\boldsymbol{u}',\end{aligned} \tag{2.10}$$

where only terms of $\mathcal{O}(\epsilon^2)$ are retained. Integration of Eq. (2.10) over Ω gives $\partial_t\|\boldsymbol{q}_c\|_T$. Due to the periodicity, the fist three terms integrate to 0, while the fourth and fifth terms are negative-definite. The last term, which is related to the compressive work, is not definite so the sign of $\partial_t\|\boldsymbol{q}_c\|_T$ cannot be concluded *a priori*.

On the other hand, considering now the Chu energy budget and retaining only $\mathcal{O}(\epsilon^2)$ terms results in

$$\rho_0\partial_t e'_c = -\boldsymbol{\nabla}\cdot(p'\boldsymbol{u}') - \frac{1}{Re}(\boldsymbol{\nabla}\cdot(\tau'\boldsymbol{u}') - \tau' : \boldsymbol{\nabla}\boldsymbol{u}') - \frac{4\gamma\mu_0 c_0}{Re\,\mathrm{Pr}}(\boldsymbol{\nabla}\cdot(c'\boldsymbol{\nabla}c') + \boldsymbol{\nabla}c'\cdot\boldsymbol{\nabla}c'), \tag{2.11}$$

where $e_c = \boldsymbol{u}'\cdot\boldsymbol{u}'/2 + A\rho'^2 + Be'^2$ is the integrand in Eq. (2.5) and $e' = 2c_0c'$ is used to compare with Eq. (2.10). Note that the viscous heating from the energy equation is not included in $\partial_t e_c$ because it is $\mathcal{O}(\epsilon^3)$ for this example. In the absence of viscosity or heat transfer, $\partial_t\|\boldsymbol{q}'_e\|_C = 0$ (Chu 1965; George & Sujith 2011). For a viscous flow with heat transfer, $\partial_t\|\boldsymbol{q}'_e\|_C \leq 0$, as was shown by Chu (1965). This simple system illustrates that $\partial_t\|\boldsymbol{q}_c\|_T$ includes compressive work terms that are, by construction, omitted in the Chu norm (Hanifi *et al.* 1996).

For certain systems, the Chu norm has desirable properties that the total energy norm does not have, namely in the negative-definiteness for the system described here. However, the total energy norm provides a measure of the space-averaged e_T, thus providing a physically relevant measure of a fluctuation's energy with quadratic terms.

2.4. *Proper orthogonal decomposition*

Here, snapshot POD is used to illustrate the differences between using the Chu norms and the total energy norms within a turbulent channel with x and z as periodic homogenous directions. First, the approach described in Moin & Moser (1989) is followed by using the instantaneous Fourier modes of the state as the snapshots. The Fourier modes, $\widehat{\boldsymbol{q}}(y,t;k_x,k_z)$, where k_x and k_z are streamwise and spanwise wavenumbers, respectively, are defined similar to those in Jiménez (2023) to ensure streamwise-aligned modes. For each k_x and k_z, a covariance matrix $\mathbf{C}(y,y';k_x,k_z)$ is defined, where $C_{ij}(y,y';k_x,k_z) = \overline{\widehat{q}_i(y,t;k_x,k_z)^*\widehat{q}_j(y',t;k_x,k_z)}$ and * denotes a complex-conjugate. Because $y \in [0,2h]$ is the only coordinate for the Fourier modes, the norms are integrated across y and $\Omega = [0,2h]$. Furthermore, the norms are now defined as $\|\widehat{\boldsymbol{q}}\|_X = \int_0^{2h} \widehat{\boldsymbol{q}}^H \mathbf{W}_X \widehat{\boldsymbol{q}} dy$, where the superscript H is a complex-conjugate-transpose and the subscript X can be C, C_2, T, or T_2 for Eqs. (2.5–2.8). Following Moin & Moser (1989), the POD modes are found as those that maximize $\lambda(k_x,k_z)$, where

$$\int_0^{2h}\int_0^{2h} \mathbf{\Phi}(y)^H \mathbf{W}_X(y)\mathbf{C}(y',y)\mathbf{W}_X(y')\mathbf{\Phi}(y')dy'dy = \lambda^2 \int_0^{2h} \mathbf{\Phi}(y)^H \mathbf{W}_X(y)\mathbf{\Phi}(y)dy, \quad (2.12)$$

and k_x and k_z are omitted for brevity. The $\mathbf{\Phi}$ that maximizes Eq. (2.12) satisfies the eigenvalue problem

$$\int_0^{2h} \mathbf{W}_X(y)\mathbf{C}(y',y)\mathbf{W}_X(y')\mathbf{\Phi}_i(y')dy' = \lambda_i^2 \mathbf{W}_X(y)\mathbf{\Phi}_i(y), \quad (2.13)$$

where λ_i are ordered in descending order, and $\mathbf{\Phi}_i$ are the orthonormal POD modes. After computing, the $\mathbf{\Phi}_i$ are re-evaluated as $\mathbf{\Phi}_i = 1/\lambda_i^2 \int_0^{2h} \mathbf{C}(y',y)\mathbf{W}_X(y')\mathbf{\Phi}_i(y')dy'$ to recover the ρ component in the total energy norm.

The integration is done through trapezoidal integration. The minimal channel used has $Ma = u_b/a_w = 1.5$, where u_b is the bulk velocity, and a_w is the speed of sound at the wall, and $Re_\tau = u_\tau h \rho_w/\mu_w = 220$. The box uses dimensions of $L_x^+ = 519$, $L_z^+ = 230$ for the streamwise and spanwise directions, $N_x = N_z = 64$ grid points for the streamwise and spanwise directions, and $N_y = 162$ wall-normal grid points. A total of 14300 snapshots saved every $\Delta t^+ = 6.7$ are used to compute the statistics. Symmetry across the channel half-height is enforced for $\mathbf{C}$.

2.5. *Resolvent analysis*

The change of variables introduced with c necessitates a new resolvent operator for an appropriately chosen norm. It will once again be assumed that the flow is homogeneous in x and z and statistically stationary. The mean state is given by $\overline{\boldsymbol{q}}_e = \overline{\boldsymbol{q}}_e(y)$ or $\overline{\boldsymbol{q}}_e = \overline{\boldsymbol{q}}_c(y)$. First, the Jacobian of the NSE with respect to state $\boldsymbol{q}_\chi$ evaluated at $\overline{\boldsymbol{q}}_\chi$ is evaluated and denoted as $\mathbf{L}_\chi$, where χ is either e or c. The governing equations can then be written as

$$(\partial_t - \mathbf{L}_\chi)\boldsymbol{q}'_\chi = \boldsymbol{f}(\boldsymbol{q}_\chi) - \mathbf{L}_\chi \boldsymbol{q}'_\chi = \boldsymbol{n}(\boldsymbol{q}_\chi), \quad (2.14)$$

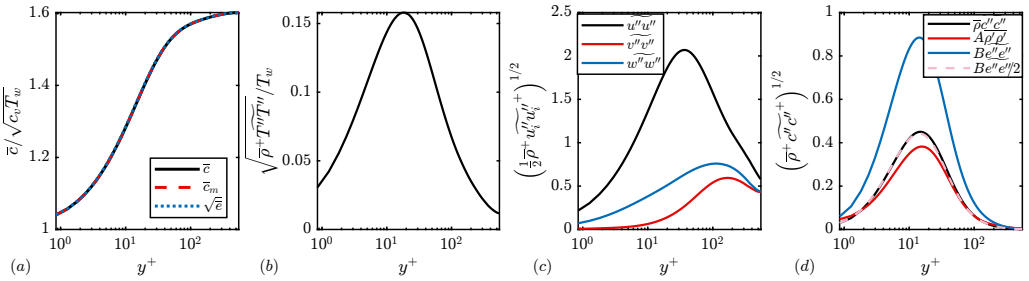

FIGURE 1. Statistics of a $Ma = 3$, $Re_\tau = 550$ isothermal channel: (a) comparison of c, c_m , and $\sqrt{e}$, (b) plots of the thermal fluctuations, (c) components of the TKE, and (d) the Chu-weighted fluctuations (red and blue) with the internal energy fluctuations (black).

where $\boldsymbol{f}$ is the NSE. This equation can then be Fourier transformed in t, x, and z by defining the Fourier modes as

$$\widehat{\boldsymbol{q}}(y;\omega,k_x,k_z) = \int \boldsymbol{q}(x,y,z,t)e^{i(-\omega t+k_x x+k_z z)}dxdzdt, \tag{2.15}$$

treating $\boldsymbol{n}$ as an external body force, and inverting to find

$$\widehat{\boldsymbol{q}}_\chi = \left(-i\omega - \widehat{\boldsymbol{L}}_\chi\right)^{-1}\widehat{\boldsymbol{n}}_\chi = \mathbf{R}_\chi\widehat{\boldsymbol{n}}_\chi. \tag{2.16}$$

Here, $\mathbf{R}_\chi$ is the resolvent operator for the state vector $\boldsymbol{q}_\chi$. Note that in general, $\mathbf{R}_e \neq \mathbf{R}_c$.

Next, by using the norms defined previously and integrating across the entire vertical domain, one can define appropriate norms for the forcing, $\widehat{\boldsymbol{n}}_\chi$, and the response, $\widehat{\boldsymbol{q}}_\chi$. Here, the forcing and response norms will be taken to be the same. Thus, one seeks the optimal forcing $\boldsymbol{\phi}_\chi$ that maximizes $\|\mathbf{R}_\chi\boldsymbol{\phi}\|_X$ such that $\|\boldsymbol{\phi}_\chi\|_X = 1$. It can be shown that the $\boldsymbol{\phi}_\chi$ that satisfies this must solve the eigenvalue problem

$$\mathbf{W}_\chi^{-1}\mathbf{R}_\chi^\dagger\mathbf{W}_X\mathbf{R}_\chi\boldsymbol{\phi}_{\chi,i} = \sigma_{\chi,i}^2\boldsymbol{\phi}_{\chi,i}, \tag{2.17}$$

where the resolvent gains, $\sigma_{\chi,i}$, are in descending order, and $\boldsymbol{\phi}_{\chi,i}$ are the forcing modes. The response modes are then $\boldsymbol{\psi}_{\chi,i} = \sigma_{\chi,i}^{-1}\mathbf{R}_\chi\boldsymbol{\phi}_{\chi,i}$. Depending on the choice of norm and state vector, the resolvent modes and gains can all be different (Karban *et al.* 2020). The discretization is described in Gomez (2024). The TBL uses finite differences with 701 points for $y \in [0, 5\delta_{99}]$, and the channel uses 251 Chebyshev points.

2.6. *A note on $\overline{e}$ and $\overline{c}$ and turbulent energetic contributions*

A challenge with the proposed norms when using a linear analysis based on $\boldsymbol{q}_c$ is that most publicly available data do not report $\overline{c}$, rather $\overline{e}$ is reported (through $\overline{T}$ and c_v). To create a useful approximation for $\overline{s}$ where $s = \sqrt{T}$, one can begin by performing a Reynolds decomposition of T and a subsequent Taylor series expansion in T' as

$$s = \sqrt{\overline{T}+T'} = \sqrt{\overline{T}}\sqrt{1+\frac{T'}{\overline{T}}} = \sqrt{\overline{T}}\left(1+\frac{1}{2}\frac{T'}{\overline{T}} - \frac{1}{8}\frac{T'T'}{\overline{T}^2} + \mathcal{O}\left(\left(\frac{T'}{\overline{T}}\right)^3\right)\right). \tag{2.18}$$

By taking an average of Eq. (2.18) the approximation for $\overline{s}$ can be given as

$$\overline{s} \approx \sqrt{\overline{T}}\left(1 - \frac{1}{8}\frac{\overline{T'T'}}{\overline{T}^2} + \mathcal{O}\left(\frac{\overline{T'T'T'}}{\overline{T}^3}\right)\right), \tag{2.19}$$

and thus $\overline{c}$ can be approximated using $\sqrt{c_v}\overline{s}$. The approximation for $\overline{c}$ can improve if higher-order statistics are reported, allowing for additional terms in Eq. (2.19), which may be relevant for hypersonic flows with strong thermal fluctuations. However, for the flows described here, the additional terms add slight differences between $\sqrt{\overline{T}}$ and $\overline{s}$. The approximation of $\overline{c}$ using Eq. (2.19) will be denoted c_m. A comparison of $\overline{c}$ and c_m for a $Ma = 3$ and $Re_\tau = 550$ full channel with $L_x = 6\pi$, $L_z = 2\pi$, $N_x = 768$, $N_z = 512$, and $N_y = 256$ is presented in Figure 1(a), where $\overline{c}$ and c_m are in agreement. Using the crude estimate of $\sqrt{\overline{e}}$ also provides an adequate approximation of $\overline{c}$ because the thermal fluctuations would contribute, at most, a .28% change to $\sqrt{\overline{e}}$ from the Taylor expansion for this supersonic data, as seen in Figure 1(b). Thus, the effect of a different mean for linearizing the NSE is expected to be small between $\boldsymbol{q}_e$ and $\boldsymbol{q}_c$ for these supersonic flows with moderate Ma (Karban *et al.* 2020).

Next, the individual components of the TKE, the Chu thermal energies, and the turbulent internal energy are presented in Figure 1(c,d). From these plots, it is clear that the streamwise turbulent fluctuations dominate the TKE. For the thermal energy contributions, the Chu thermal energy terms contribute a significant portion to the total Chu-defined energy. While smaller, the turbulent internal energy contributes a proportion similar in magnitude to the wall-normal contributions to the TKE. From these plots and the norm defined in Eq. (2.6), it is evident that the Chu energy overemphasizes the thermal energy terms from the natural total energy.

3. Results

This section discusses the results of POD and resolvent analysis using the different state vectors and norms. The POD is applied to the supersonic minimal flow unit described in Section 2.4. Resolvent analysis is applied to the supersonic channel described in Section 2.6 and the $Ma = 4$, $Re_\tau = 500$ supersonic TBL of Bernardini & Pirozzoli (2011). The channel data used here are computed using the Hypersonic Task-based Research (HTR) solver (Di Renzo *et al.* 2020). The TBL results without a + subscript are normalized with $\ell_s = \delta_{99}$ and freestream-evaluated scales.

3.1. *Application to POD*

The POD is applied to the time series of $\widehat{\boldsymbol{q}}_e$ and $\widehat{\boldsymbol{q}}_c$ for $k_x = 0$ and $k_z = 4\pi/L_z$ using the Chu norms and the total energy norms. Since this is a minimal channel, $k_x = 0$ encompasses any mode longer than $L_x^+ = 519$ with spanwise width of 115 viscous units. These modes are representative of the near-wall cycle and thus are expected to primarily be driven by the velocity fluctuations. The POD modes and eigenvalues are plotted in Figure 2. Note that these terms are weighted so that each panel presents the contribution to the respective norm. For the total energy norm, $\Phi_{\rho,i}$ is weighted by the density weight in $\mathbf{W}_C$ or $\mathbf{W}_{C_2}$ since otherwise the contribution would be zero from $\mathbf{W}_T$ or $\mathbf{W}_{T_2}$. The velocity components are only slightly affected by the different norm and change in state variables. For the internal energy components, the traditional Chu norm with $\widehat{\boldsymbol{q}}_e$ produces the largest component followed by the Chu norm using $\widehat{\boldsymbol{q}}_c$. The smaller contribution from the total energy norms reflect that the Chu norm uses twice the internal energy contribution than the total energy norm. Comparing the density components, once again the Chu norm with $\widehat{\boldsymbol{q}}_e$ produces the largest contribution. The observations for the leading POD mode are also shared with the third POD mode. This follows in the POD eigenvalues, where the total energy norm produces smaller eigenvalues. Even if the

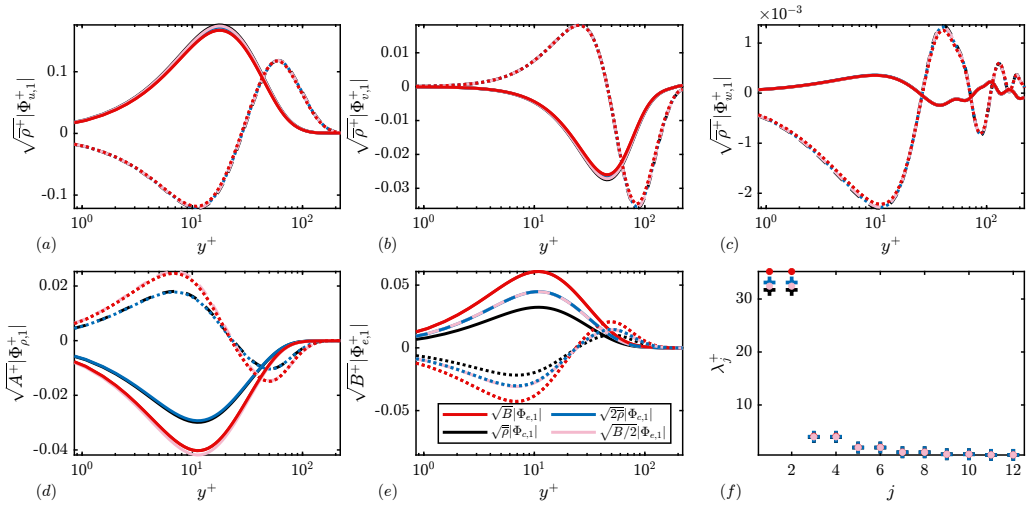

FIGURE 2. (a–e) Real parts of the components of the first (solid) and third (dashed) POD mode weighted by the norm coefficients for a $Ma = 1.5$, $Re_\tau = 220$ minimal channel for $k_x = 0$ and $k_z = 4\pi/L_z$ and (f) the POD eigenvalues. The plots are color coded following Table 1.

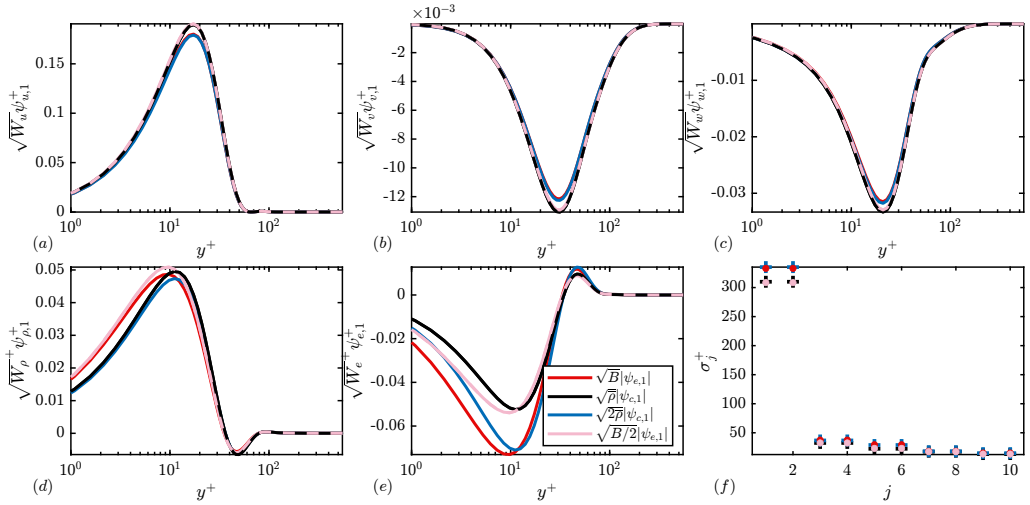

FIGURE 3. (a–e) Real parts of the components of the leading response mode weighted by the norm coefficients for a $Ma = 3$, $Re_\tau = 550$ full channel for $k_x^+ = 2\pi/1000$, $k_z^+ = 2\pi/250$, $\omega^+ = 2\pi/100$ and (f) the leading resolvent gains. The plots are color coded following Table 1.

different state vectors use the same norm, the POD modes and gains are different. This occurs because the $\widehat{c}$ and $\widehat{e}$ are different signals due to the nonlinear change in variables. Indeed, because $e = c^2$, $\widehat{e}(y,t;k_x,k_z) = \sum_{k_x',k_z'} \widehat{c}(y,t;k_x',k_z'\widehat{c}(y,t;k_x - k_x', k_z - k_z')$. This along with the different norm weights cause differences in the POD modes, primarily in the thermodynamic components.

3.2. *Application to resolvent analysis*

First, the resolvent analysis of a $Ma = 3.0$, $Re_\tau = 550$ supersonic channel is presented to highlight the near-wall response modes and gains. The resolvent response modes and

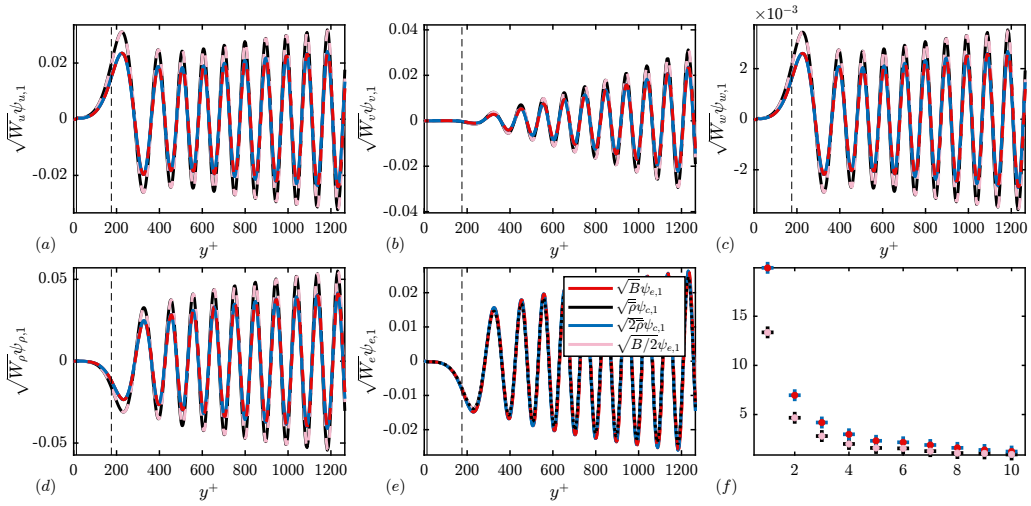

FIGURE 4. (a–e) Real parts of the components of the leading response mode weighted by the norm coefficients for a $Ma = 4$, $Re_\tau = 500$ TBL for $k_x = 3\pi$, $k_z = \pi/3$, and $\omega^+ = k_x/2$ and (f) the leading resolvent gains. The plots are color coded following Table 1. The solid vertical line is the critical layer location, y_c, such that $\overline{u}(y_c) = \omega/k_x$, and the dashed vertical line is the relative sonic line location, y_s, such that $\overline{Ma}(y_s) = 1$ where the modes are phase-matched.

gains for a $k_x^+ = 2\pi/1000$, $k_z^+ = 2\pi/100$, and $\omega^+ = 2\pi/100$ mode are presented in Figure 3, comparing the different norms and the different state vectors. The modes are weighted similarly to those in Figure 2(a–e). Similar to the results of the POD modes, the velocity components are almost indistinguishable despite the different norms and state vectors used. Furthermore, the temperature contributions to the mode are largest for the Chu norm using $\widehat{\boldsymbol{q}}_e$ and smallest for the total energy norm using $\widehat{\boldsymbol{q}}_c$. In the region closest to the wall, the mode shapes and amplitudes differ most substantially for the e or c components. This may stem from changes to the linearized equations by introducing the change of variables, which introduce different weightings to the temperature gradients (Karban *et al.* 2020). For the modes shown here with different state vectors, the σ_i are almost identical when using the same norm. The Chu norms attain larger σ_i than the total energy norms due to the aforementioned increased weighting of the thermodynamic components.

Since the POD modes and the resolvent mode plotted in Figure 3 are representative of near-wall dynamics, it is expected that these modes are driven primarily by hydrodynamic components. Thus, for the remainder of this section, the analysis now focuses on acoustic modes by considering the $Ma = 4$, $Re_\tau = 500$ TBL. Acoustic resolvent modes are excited by the proximity of $-i\omega$ to eigenvalues corresponding to freestream Mack modes (Mack 1984), which are excited when the local relative Mach number,

$$\overline{Ma} = \frac{k_x}{\sqrt{k_x^2 + k_z^2}} \frac{Ma(\overline{u} - \omega/k_x)}{\sqrt{\overline{T}}} = \frac{k_x}{\sqrt{k_x^2 + k_z^2}} \frac{(\overline{u} - \omega/k_x)}{\sqrt{\gamma(\gamma - 1)\overline{e}}}, \tag{3.1}$$

is greater than 1. This causes the resolvent modes to experience discontinuous behavior across the sonic line in spectral space where $\overline{Ma}(k_x, k_z, \omega) = 1$ (Bae *et al.* 2020).

Because these modes radiate freestream acoustics, they are strongly influenced by the compressible phenomena and as a result may be more sensitive to the choice of norm. For instance, Section 2.2 demonstrated that the Chu norm weighs the thermodynamic components of acoustic Kovasznay (1953) modes 7 times what the total energy norm

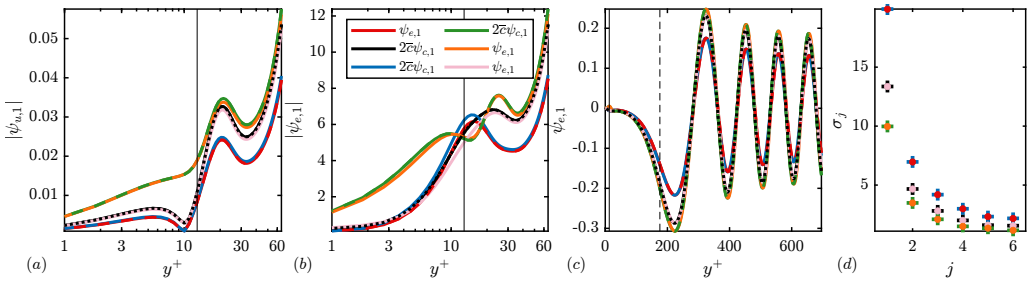

FIGURE 5. (a,b) Magnitude of the modes computed in Figure 4 including the kinetic energy modes in the near-wall region. (c) Full view of the real part of $\psi_{e,1}$. The solid vertical line is y_c and the dashed vertical line y_s. (d) The leading resolvent gains.

does. Here, a relatively supersonic mode is considered with $k_x = 3\pi$, $k_z = \pi/3$, and $\omega = k_x/2$ resulting in a $\overline{Ma} = 2$ in Figure 4, where the modes are again weighted by the components of the respective norms. Unlike the near-wall modes presented before, this acoustic phenomenon is now much more affected by the choice of norm, though only slightly affected by the choice of state variable. When the modes are calculated using the same norm, the gains are indistinguishable, differing by less than a percent. Using the total energy norm results in smaller amplification in line with the previous observations. The velocity contributions from the total energy norm have larger magnitudes than those from the Chu norm, while the temperature components are identical. While the density contribution is not included in the total energy norm, it is interesting to note that some of the contributions from the velocity have been transferred to the density component in the Chu norm.

Finally, the modes and gains computed with the kinetic energy norm for the supersonic mode highlighted in Figure 4 are included in Figure 5. Since the modes computed with the state vector $\widehat{\boldsymbol{q}}_c$ do not have an e component, the e component is computed as $\psi_{e,i} = 2\bar{c}\psi_{c,i}$ through a linearization of e that agrees well with $\psi_{e,i}$ when computed using the same norm. Figure 5(a,b) highlights the differences in the near-wall region between the different norms used. The kinetic energy norms are indistinguishable despite the different state vectors, just like those using the Chu norm. The different norms affect primarily the near-wall region far away from the freestream where the acoustic phenomenon takes hold. Away from the wall, the e components have a similar structure due to the acoustic mode excitation. The only differences are in the amplitudes where the kinetic energy norm produces the largest $\psi_{e,1}$ because e is not constrained. This is followed by the total energy norm and ultimately the Chu norm. The smaller amplitude is because the Chu norm effectively double counts the internal energy contribution. Finally, σ_i is smaller for the kinetic energy norm because it omits the thermal energy.

3.3. *Implications for flow reconstruction and modeling*

A challenge with working with c rather than e is that most studies report and store statistics of e (or equivalently T) rather than c. Furthermore, thermal fluctuations are often more desirable to model than fluctuations of $\sqrt{T}$. Nonetheless, the comparisons made between ψ_e and $2\bar{c}\psi_c$ in Figure 5 show promise in applying this change of variables to reconstruct thermal statistics. The strong resemblance between the modes computed using either the Chu norms or the total energy norms suggests that any flow reconstruction strategy using the Chu norm can easily be applied to the total energy norm modes. This will be a topic of future studies. While in a data-driven setting, it is possible to

trivially switch between $\boldsymbol{q}_e$ and $\boldsymbol{q}_c$, an equation-driven setting requires a new discretization of the linearized or modeled equations. However, the similarity between using c' and $c' = e'/(2\overline{e})$ and the norm in Eq. (2.8) is encouraging because it enables the total energy-maximizing properties of working with c' without the need for a new derivation, allowing for quick application to existing tools.

4. Conclusions and future work

A new L_2 norm is proposed that has the interpretation of being a turbulent total energy by introducing the variable $c = \sqrt{e}$. Here, the application of this norm to POD and resolvent analysis is discussed and compared with classically used Chu energy norms. Because of the change of variables, this necessitates a new linearization of the NSE. It is shown that despite the differences in the linear operator, when using the same norm, the results are almost indistinguishable for moderate Ma. However, using the total energy consistently results in less amplification than the Chu energy norms.

Since the linear analysis demonstrates more substantial differences between the norms in freestream acoustics, future work will consider the total energy norm as an alternative to the Chu norm for jet noise applications. Because of the parallels Fan *et al.* (2022) observed between the kinetic energy and internal energy budgets using c, such parallels can be investigated for nonlinear closure to represent $\widehat{\boldsymbol{q}}_c$ with the spatial modes described here and to understand the modal energy exchanges.

The small differences in the linearizations stem from $\overline{c}$ and $\sqrt{\overline{e}}$ being almost equivalent. For moderate Ma, it was shown that using a linearization of c allows the application of the total energy norm to linear studies using $\boldsymbol{q}_e$ without the need for a change of variables, enabling quick application of this norm to existing linear analyses. It is likely that for hypersonic flows with larger $\sqrt{\overline{T'T'}}$ relative to $\overline{T}$, differences can become more appreciable in the linearizations. The different linearizations and new disturbance energy growth can have strong implications for transient growth analyses in hypersonic flows. The total energy norm can lead to improved predictions in hypersonic transition to turbulence by optimizing a norm that measures a fluctuation's total energy and accounts for the compressive work in its temporal evolution. This norm can be applied to any SVD-based approach in compressible flows, which includes popular methods like POD, SPOD, linear transient growth, and resolvent analysis.

Acknowledgments

The support of ONR to CTR under grant N000142312833 is gratefully acknowledged. S. R. G. thanks Christopher Williams for his insightful comments and thorough review of this brief and Dr. Akhil Nekkanti for fruitful discussions as this brief was prepared.

REFERENCES

Bae, H. J., Dawson, S. T. & McKeon, B. J. 2020 Resolvent-based study of compressibility effects on supersonic turbulent boundary layers. *J. Fluid Mech.* **883**, A29.

Berkooz, G., Holmes, P. & Lumley, J. L. 1993 The proper orthogonal decomposition in the analysis of turbulent flows. *Annu. Rev. Fluid Mech.* **25**, 539–575.

Bernardini, M. & Pirozzoli, S. 2011 Wall pressure fluctuations beneath supersonic turbulent boundary layers. *Phys. Fluids* **23**.

Chu, B.-T. 1965 On the energy transfer to small disturbances in fluid flow (Part I). *Acta Mech.* **1**, 215–234.

Di Renzo, M., Fu, L. & Urzay, J. 2020 HTR solver: an open-source exascale-oriented task-based multi-GPU high-order code for hypersonic aerothermodynamics. *Comput. Phys. Commun.* **255**, 107262.

Fan, Y. & Li, W. 2023 Spectral analysis of turbulence kinetic and internal energy budgets in hypersonic turbulent boundary layers. *Phys. Rev. Fluids* **8**, 044604.

Fan, Y., Li, W. & Pirozzoli, S. 2022 Energy exchanges in hypersonic flows. *Phys. Rev. Fluids* **7**, L092601.

George, K. J. & Sujith, R. 2011 On Chu's disturbance energy. *J. Sound Vib.* **330**, 5280–5291.

Gomez, S. R. 2024 *Linear amplification in nonequilibrium turbulent boundary layers*. Doctoral dissertation, California Institute of Technology.

Hanifi, A., Schmid, P. J. & Henningson, D. S. 1996 Transient growth in compressible boundary layer flow. *Phys. Fluids* **8**, 826–837.

Jiménez, J. 2023 A Perron–Frobenius analysis of wall-bounded turbulence. *J. Fluid Mech.* **968**, A10.

Karban, U., Bugeat, B., Martini, E., Towne, A., Cavalieri, A., Lesshafft, L., Agarwal, A., Jordan, P. & Colonius, T. 2020 Ambiguity in mean-flow-based linear analysis. *J. Fluid Mech.* **900**, R5.

Kovasznay, L. S. 1953 Turbulence in supersonic flow. *J. Aeronaut. Sci.* **20**, 657–674.

Lumley, J. L. 1967 The structure of inhomogeneous turbulent flows. In *Atmospheric turbulence and radio wave propagation* (pp. 166–178). Nauka.

Mack, L. M. 1984 Boundary-layer linear stability theory. *Tech. Rep.*, Jet Propulsion Lab, California Institute of Technology.

McKeon, B. J. & Sharma, A. S. 2010 A critical-layer framework for turbulent pipe flow. *J. Fluid Mech.* **658**, 336–382.

Mettot, C., Renac, F. & Sipp, D. 2014 Computation of eigenvalue sensitivity to base flow modifications in a discrete framework: application to open-loop control. *J. Comput. Phys.* **269**, 234–258.

Moin, P. & Moser, R. D. 1989 Characteristic-eddy decomposition of turbulence in a channel. *J. Fluid Mech.* **200**, 471–509.

Picard, C. & Delville, J. 2000 Pressure velocity coupling in a subsonic round jet. *Int. J. Heat Fluid Flow* **21**, 359–364.

Schmid, P. J. & Henningson, D. S. 2001 *Stability and Transition in Shear Flows* (AMS, Vol. 142). Springer.

Schmidt, O. T., Towne, A., Rigas, G., Colonius, T. & Bres, G. A. 2018 Spectral analysis of jet turbulence. *J. Fluid Mech.* **855**, 953–982.

Sieber, M., Paschereit, C. O. & Oberleithner, K. 2016 Spectral proper orthogonal decomposition. *J. Fluid Mech.* **792**, 798–828.

Taira, K., Brunton, S. L., Dawson, S. T., Rowley, C. W., Colonius, T., McKeon, B. J., Schmidt, O. T., Gordeyev, S., Theofilis, V. & Ukeiley, L. S. 2017 Modal analysis of fluid flows: an overview. *AIAA J.* **55**, 4013–4041.

Towne, A., Schmidt, O. T. & Colonius, T. 2018 Spectral proper orthogonal decomposition and its relationship to dynamic mode decomposition and resolvent analysis. *J. Fluid Mech.* **847**, 821–867.